Monte Carlo Simulation of Uniaxial Tension of an Amorphous Polyethylene-like Polymer Glass

Jing Li,[†,‡] Tim Mulder,*,[‡] Bart Vorselaars,[‡] Alexey V. Lyulin,[‡] and M. A. J. Michels[‡]

Department of Macromolecular Science and Key Lab of Molecular Engineering of Polymers, Ministry of Education of China, Fudan University, Shanghai 200433, China, and Group Polymer Physics, Eindhoven Polymer Laboratories and Dutch Polymer Institute, Technische Universiteit Eindhoven, P.O. Box 513 5600 MB Eindhoven, The Netherlands

ABSTRACT: Atomistic Monte Carlo (MC) simulations of uniaxial tension of an amorphous linear polyethylene (PE)-like polymer glass have been carried out. A united-atom model has been used where PE chains are represented by beads connected by flexible springs. Highly efficient end-bridging MC moves have been used to first equilibrate the polymer in the melt and then cool to a temperature below its glass transition temperature. A mix of efficient MC moves has also been used to simulate the deformation dynamics. Upon uniaxial deformation the stress response to the strain is initially linear elastic, subsequently as the strain increases further yielding is observed, and finally strain hardening is developed. The simulated Young modulus and Poisson ratio take realistic values. Furthermore, the temperature and strain rate dependencies of stress−strain curves have been investigated, and the results are in qualitative agreement with the experimental observations. Chain conformation and energy and stress partitioning with increasing strain are followed in detail. During the deformation the chains adopt more extended conformations, and the fraction of dyads in the trans state increases. In the elastic region mechanical work done on the sample is primarily stored as nonbonded internal energy, whereas from the yield region onward the intrachain contributions start to play a role.

1. Introduction

A long-standing problem in polymer science concerns the mechanical behavior of glassy amorphous polymers under deformation. Numerous experimental and theoretical efforts have been put on investigating elastic response, yielding (the stress stops increasing with strain at the onset of yielding), strain softening (a drop in the yield stress with strain), and strain hardening (the steep increase of the stress with strain at large strain values). It is found that the yield stress increases with increasing strain rate, decreasing temperature, and increasing pressure;[1] the postyield strain-hardening behavior is found to strongly depend on the state of deformation[2] and involves also the cross-linked or entangled polymer network which is loaded at large strains.[3] Nevertheless, the direct connection between the network density and strain-hardening modulus and the physical origin of strain softening are not well understood.[3]

Molecular simulations provide a route to investigate polymers at the molecular level and thus to obtain more detailed information on the static and dynamic properties than can be extracted from experimental measurement. Molecular dynamics (MD) and Monte Carlo (MC) have proved to be successful tools for exploring the structure and properties of bulk amorphous polymers at the molecular level. One of the first detailed MD computer simulations of an amorphous polyethylene-like polymer under uniaxial tension was performed by Brown and Clarke[4] in 1991. They prepared initial samples of 1000 united atoms which after equilibration at melt temperature are cooled at a rate of 10^{12} K s^{-1} and subsequently equilibrated for 1 ns. Thereafter, uniaxial deformation was simulated with various tension rates (corresponding to deformation rates of the order of 10^9 s^{-1}). A loose coupling constant-pressure molecular dynamics simulation was carried out for times up to 1 ns. The

simulated elastic deformation, yield, and plastic flow at low temperatures show similarity with laboratory results obtained on time scales that are many orders of magnitude longer. Despite problems such as a small system size and huge cooling and deformation rates, MD has proved to be a useful tool in studying deformation behavior of amorphous polymers. Capaldi et al.[5] for instance studied, in 2004, the behavior of a glassy PE-like polymer undergoing active compressive deformation by MD. They found that deformation increases the transition rate between different dihedral angle states and promotes propagation of dihedral angle flips along the chain. Recently, Lyulin et al.[6] showed that it was possible to simulate by MD both glassy atactic polystyrene and glassy bisphenol A polycarbonate, using chemically realistic models, under uniaxial mechanical deformation, employing a deformation rate of 10^8 s^{-1}. The initial samples were cooled from the melt at a speed of 10^{12} K s^{-1}. It was shown that the simulated Young moduli, yield stresses, and strain-hardening moduli were in fair agreement with existing experiments. An important observation is that the mobility of the PS segments in the deformation direction is increased drastically beyond the yield point. A weaker increase is observed for PC.

Apart from limitations mentioned above, a serious drawback of MD simulations is the problem of preparing well-equilibrated initial samples at melt temperature. Typically chains are first generated by some (self-avoiding) random-walk process and subsequently equilibrated by MD.[4,7,8] However, the equilibration achieved in such a simulation is far from complete. The longest relaxation time rapidly increases with chain length; even for relatively short chains (a few tens of monomers) the longest relaxation time will exceed the accessible computer time. As a consequence, the large-scale configurational characteristics of the polymer system will hardly evolve, and the system will remain close to its initial position in phase space. The result is an inefficient sampling of phase space and unreliable estimations

[†] Fudan University.
[‡] Technische Universiteit Eindhoven.

of both statistical and dynamical properties. In some cases use has been made of MC simulations for sample equilibration. Capaldi et al.,[5] for example, used MC with single-atom-displacement moves for equilibration. The local nature of this kind of moves does not solve the equilibration problem either. In due time lots of efforts have been made in improving upon the situation at hand by developing advanced MC moves. Vacatello et al.[9] introduced the "reptation" (REP) move, where a monomer is cut off from a randomly selected chain end and subsequently attached to the other end of the same chain. In a so-called "configurational bias" (CB) move,[10] a randomly selected chain is cut in two pieces, one of which is removed and then regrown segment by segment, avoiding overlap with surrounding segments. Dodd et al.[11] came up with the "concerted rotation" (CONROT) move, where one trimer is excised from a chain, the two adjacent atoms are displaced by changing their dihedral angles, and finally the trimer is placed in between the adjacent atoms (at their new positions). In the 1990s it appeared possible with these moves to fully equilibrate polymer chains up to 30 monomers. For longer chains descriptors such as the end-to-end distance vector did not completely forget the values they had in the beginning of the simulation.[12,13] A real breakthrough came when Pant and Theodorou[14] introduced their so-called "end-bridging" MC move. This move, which alters the connectivity of chains, made very large steps in phase space possible. The long relaxation times that scale with the degree of polymerization could be circumvented.

Besides equilibration, the energy-based MC method appeared to be a useful tool in the study of nonequilibrium dynamical processes, such as polymer deformation, as well. Typically in such simulations one type of move is used, and an estimate is made of the corresponding time scale. Wittkop et al.[15] used lattice Monte Carlo (MC) simulations to study the deformation behavior of a bond-fluctuation polymer-chain model under an external force in 2D and 3D and found a good agreement in the chain end-to-end distance over a large force range between simulation results and theoretical estimations. Hölzl[16] used MC simulations employing the same lattice model to investigate deformation of polymer melts and observed that the sample significantly shrinks laterally near the glass-transition temperature. Below T_g voids are produced and chains are extremely stretched. Recently, Ospina et al.[17,18] simulated by MC the initial stage of deformation of linear polyethylene (PE) using a 2D lattice model and observed a stress–strain behavior comparable to what is observed in experiments,[19] but neither strain softening nor strain hardening was reported. 3D off-lattice MC simulations of PE-like cross-linked networks have been performed recently by Chui and Boyce[1] to study the mechanical-deformation process under various loading conditions. Their model has been found to qualitatively capture the rate and temperature dependence of deformation observed experimentally for real amorphous polymeric materials. Chui and Boyce perform a careful study of the separate contributions of the nonbonded as well as the various bonded interactions to both the internal energy and the stresses. Their main conclusions are that the strain softening is a result of the evolution of intermolecular contributions to the response whereas the strain-hardening phenomenon is a result of evolution in the intramolecular contributions. Chui and Boyce used one type of (local) MC move, in which one particle is selected at random and its position is perturbed by a small random displacement. They estimate that, by using these very local moves, the deformation rate in their simulations equals 10^8–10^9 s^{-1}.

Here an MC study is reported to investigate the uniaxial tension (up to 80% strain) of an amorphous non-cross-linked PE-like glass. Special attention is given to producing well-equilibrated initial samples by employing advanced MC moves that enable equilibration at the time scale of the longest relaxation times. Subsequently, deformation of the polymer samples is simulated with MC at an estimated deformation rate of 10^8 s^{-1} or slower.

Extensive simulations, using advanced MC moves such as REP, CONROT, and EB moves, have been performed to prepare well-equilibrated initial samples of 5000 monomers in the melt. Especially EB had proved to be of great help in efficiently sampling the configuration space of systems of long-chain polymers. After subsequent cooling, we used MC to simulate the uniaxial tensile deformation of PE by employing efficient local moves, primarily CONROT. By doing so, it should be possible to obtain effective deformation rates that are lower than so far achieved in simulations; in the present implementation we estimate our rates to be about 10^8 s^{-1}. To validate our simulations, properties such as stress–strain behavior and its dependence on temperature and strain rate have been studied to check whether experimental dependencies are at least qualitatively reproduced. As an extra check we have studied the calorimetric behavior and compared the results to experimental data from Hasan and Boyce.[20] Subsequently, following Chui and Boyce, to obtain insight into the role of the different bonded and nonbonded interactions during deformation, the evolution of contributions from the different interactions to internal energy and internal stress, at various stages of the deformation process, has been investigated. In addition, the evolution of chain conformations has been examined and compared to previous simulations.[1,5,21]

In section 2 the PE model, the details of the MC algorithms, the different types of moves used in the present study, and details of the stress calculations are explained. The equilibration and cooling are elaborated on in section 3. In section 4 the stress–strain relations are discussed. Subsequently, the evolution of the internal energy contributions upon deformation is treated, together with the evolution of chain conformations. Finally, in section 5, conclusions are drawn.

2. PE Model and Simulation Algorithm

We studied a united-atom model of linear PE, where each CH$_2$ group is considered as a bead and each chemical bond on the backbone is represented by a spring via a harmonic bond stretching potential U_l. The valence angle is governed by a harmonic angle bending potential U_θ. The Ryckaert–Bellemans torsional potential U_ϕ[22] is used, and interactions between beads on different chains and beads separated by more than three bonds on the same chain are described by the Lennard-Jones potential. The exact functional forms and values of the parameters associated with these potentials are given in Table 1. The Lennard-Jones potential is truncated at 2.3σ, and a quintic spline was used from 1.45σ to 2.3σ;[23] long-range interactions are left out since no attempt is made to compare the results accurately with experimental values.

The equilibrium internal stress tensor of a periodic monatomic system can be calculated using the expression[24,25]

$$\tau^{\alpha\beta} = \left\langle -\frac{1}{V}\sum_i \frac{p_i^\alpha p_i^\beta}{m_i} - \frac{1}{2V}\sum_i\sum_j (r_i^\alpha - r_{j_{min}(i)}^\alpha)F_{ij}^{min,\beta} \right\rangle + \tau_{tail}^{\alpha\beta} \tag{1}$$

where $\tau^{\alpha\beta}$ is the $\alpha\beta$ component of the stress, V is the system

Table 1. Force Field[a]

interaction type	functional form	parameters
bond stretching	$U_l = \frac{1}{2}k_l(l - l_0)^2$	$k_l = 1674$ kJ Å^{-2} mol^{-1}, $l_0 = 1.54$ Å
angle bending	$U_\theta = \frac{1}{2}k_\theta(\theta - \theta_0)^2$	$k_\theta = 481.8$ kJ rad^{-2} mol^{-1}, $\theta_0 = 1.955$ rad
torsion	$U_\phi = \sum_{k=0}^{5} c_k \cos^k(\phi)$	$c_0 = 9.279$ kJ mol^{-1}, $c_1 = 12.16$ kJ mol^{-1}, $c_2 = -13.12$ kJ mol^{-1}, $c_3 = 3.060$ kJ mol^{-1}, $c_4 = 26.24$ kJ mol^{-1}, $c_5 = 31.49$ kJ mol^{-1}
nonbonded	$U_{LJ} = 4\epsilon[(\sigma/r)^{12} - (\sigma/r)^6]$	$\epsilon = 0.410$ kJ mol^{-1}, $\sigma = 3.94$ Å

[a] Parameter values are taken from ref 13, except the value of the bond stretching potential k_l, which is taken from ref 1.
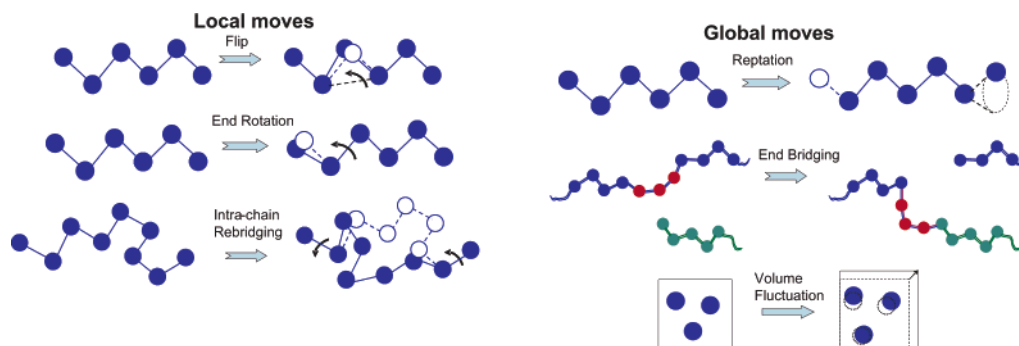

Figure 1. Local MC moves (left) and global MC moves (right) implemented in the present study.

volume, and p_i^α is the α component of the momentum of site i with mass m_i. $\mathbf{r}_i$ is the position vector of site i, $j_{\min}(i)$ denotes the minimum image of site j with respect to site i, and $\mathbf{F}_{ij}^{\min}$ is the force on i due to the interaction with $j_{\min}(i)$. τ_{tail} in eq 1 is a tail contribution from the interactions U_{tail} beyond the potential cutoff distance, which are neglected in the present study.

In a system of polyatomic molecules, $\mathbf{F}_{ij}$ includes nonbonded forces from the excluded-volume interactions and bonded forces from the bonds, the valence angles, and the dihedral angles. It was pointed out in refs 25 and 26 that the contribution of valence angles and dihedral angles to the trace of the instantaneous value of the stress tensor is zero. In other words, the pressure is governed only by the nonbonded forces and the bond stretching forces. However, valence angle and torsional forces do affect the instantaneous values of the individual normal as well as shear stresses in the system. The momentum term on the right-hand side of eq 1 cannot be calculated directly in an MC simulation. However, for equilibrium situations it is often assumed that on-diagonal elements of the kinetic part of the stress tensor are simply related to temperature and that off-diagonal elements are zero; that is, the kinetic term can be written in terms of the system temperature as $\langle -N/V \rangle k_B T \delta_{\alpha\beta}$, where N is the total number of monomers in the periodic box and $\delta_{\alpha\beta}$ the Kronecker delta.[25] In this study we go one step further in that eq 1 is used during deformation (nonequilibrium simulations) as well. The internal pressure in the present MC simulations is calculated as the negative trace of the stress tensor in eq 1.

PE chains are contained in an orthorhombic box, which starts (before deformation) as a cubic box of size 50 Å, with periodic boundary conditions. (Although simple to implement, orthorhombic periodic boundary conditions do not allow one to control or respond to off-diagonal components of the stress. However in our study we observed that the off-diagonal elements are very small and equal to each other within the statistical errors.) The chain length distribution is uniform in the interval from $\bar{X}(1 - \Delta)$ to $\bar{X}(1 + \Delta)$, where $\bar{X}$ is the number-average degree of polymerization and Δ the half-width of the chain length distribution reduced by the number-average chain length. A geometrical builder is used to create initial PE samples of 5000 monomers with $\bar{X} = 50$ and $\Delta = 0.5$. (Preliminary results on

longer chain systems, for example $\bar{X} = 500$ and $\Delta = 0.5$, resulted in the same qualitative picture of deformation.) The initial temperature is 450 K. During this sample-building process hard-sphere overlap is prevented.

In the present study six types of moves have been used: three local and three global types of MC moves (see Figure 1). During a "flip" move, a trimer in the middle of a chain is selected at random, and subsequently the apex atom is rotated by a small angle along the line connecting the two neighboring atoms, which are kept fixed in the move. During an "end rotation" move a chain end (start) is selected at random, and the last segment is rotated around the neighboring bond by changing the torsional angle defined by the last (first) four beads of the chains. The "intrachain rebridging" or "concerted rotation" (CONROT) move as well as the REP move has been explained before. To efficiently apply the MC technique to a long-chains polymer melt, Theodorou et al.[13,23] developed the connectivity-altering EB MC move. During an EB move, two melt chains are selected so that the end of one is within a certain bridgable distance from a backbone segment of the other. A trimer centered at this latter backbone segment is excised from the second chain, thus defining two subchains. The end of one of these subchains is connected to the end of the first chain by constructing a bridging trimer, forming a new chain with prescribed molecular geometry (bond lengths and bond angles). Clearly, the EB move alters the lengths of chains participating in it. To control the chain-length distribution, any trial move which makes the length of any chain fall outside the prescribed range of chain lengths is immediately rejected. Finally, a "volume fluctuation" move modifies simultaneously the box sizes in all directions i ($i \in x, y, z$) affinely with the coordinates of all atoms: the box size L is increased by ΔL and the i-coordinate $i(j)$ of the position of a site j is shifted by $\Delta i(j) = \Delta L[(i(j) - i_0)]/L$, with i_0 the position of the face of the box that keeps its position (the opposite face is displaced ΔL in the i-direction).

The initial PE samples are first equilibrated in the NPT ensemble at melt temperature $T = 450$ K and isotropic external pressure $P = 0.1$ MPa. The question of the equilibration of a (nondeformed) PE melt was given special attention in the present study. A mix of MC moves with different attempt probabilities

is used, similar to the mix of moves used by Mavrantzas et al.:[13] 6% reptation, 6% end rotation, 6% flip, 32% intrachain rebridging, 49% end-bridging, and 1% volume fluctuation. This choice was made in order to make especially the end-bridging move efficient. To obtain such efficiency the "shuttling effect", i.e., the occurrence of successive accepted EB moves that annihilate each other by performing transitions twice, in forward and backward direction, has to be reduced as much as possible. This can be done by considerably updating, between two end-bridging moves, the lists of chain ends and the backbone segments in other chains to which they can bridge.[27] It is observed that at 450 K the energy and the density achieve equilibrium values after 4×10^4 MCS, where 1 MCS (Monte Carlo step) is the number of moves divided by the total number of monomers in the system. After this initial equilibration the sample is further cooled to 100, 200, and 300 K, at a rate of 1 K every 20 MCS until it reaches the desired temperatures. It is difficult to give an estimate for the time scale of the cooling process. Above the glass transition one could claim that one cools on the time scale of the slowest processes by using the EB move, i.e., on the scale of the disengagement time (quasi-statically). As soon as the system becomes glassy, only local moves have a nonnegligible chance of acceptance. In the latter case we estimate the cooling rate to be 10^{11} K s^{-1}. Then the equilibration has been continued with the temperature fixed at its target value until the energy and the density reach stable values.

The equilibrated samples at different temperatures and at atmospheric pressure ($P = 0.1$ MPa) are uniaxially deformed at constant effective velocity in the z-direction: the box size L_z is increased by $\Delta L_z = 0.1$ Å every 100–200 MCS. All positions of sites in the box are scaled affinely with the box size, i.e., $\Delta z = \Delta L_z[(z - z_0)/L_z]$, where z is the position of a site and z_0 the position of the face of the box that keeps its position (the opposite face is displaced ΔL_z in the z-direction). Besides a "lateral size fluctuation" move (comparable to the volume fluctuation move) that modifies simultaneously the box sizes in directions x and y, during deformation only local moves (primarily the CONROT move) are used, to avoid a direct intervening in the slowest processes (that take place on time scales that also exceed experimental time scales of the order of seconds or larger). The exact mix of moves is 55.88% CONROT, 34% flip, 10% end rotation, and 0.12% lateral size fluctuation. We use as estimate for the time corresponding to one MCS (one Monte Carlo step per monomer), the time in which the MSTD (mean-square translational displacement) of a monomer in a united-atom MD simulation of PE equals the average bead displacement due to a typical CONROT move (average of a few tens of CONROT moves). This time is $\sim 10^{-13}$ s. This would imply a deformation rate of the order of 10^8 s^{-1}. However, since the time estimate is very crude, it is dangerous to draw final conclusions regarding cooling rates or deformation rates.

3. Preparation of the Initial Polymer Melt

3.1. Equilibration at 450 K. During the initial equilibration the energy and the density of a PE sample are calculated every move, while the stress is calculated at every 20 MCS. The density evolution in Figure 2a shows the fast equilibration of the sample by the MC algorithms. Within 2×10^3 MCS the system evolves to an equilibrium density of 0.81 g cm^{-3}. As the purpose of the present study is not to reproduce the experimental density, the parameters of the implemented force fields are not carefully calibrated vs the available experimental results. Similar to the density, the energy also reaches equilib-
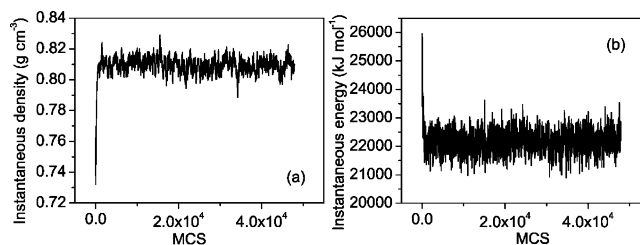
Figure 2. Density (a) and total energy (b) evolution during the equilibration of the initial samples at 450 K and 0.1 MPa. Results are plotted every 20 MCS. The average equilibrium density and energy of the initial samples are 0.81 g cm^{-3} and 22.1×10^3 kJ mol^{-1}.
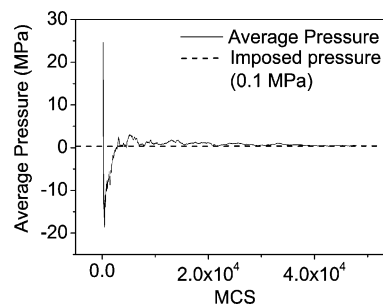
Figure 3. Average pressure (average of all values from the move at which the monitoring was started, after 200 MCS, until the last move performed) obtained from the equilibration of the initial PE sample at 450 K and 0.1 MPa. Results are plotted every 20 MCS.

Table 2. Comparison of the Pressure Contributions from Different Types of Interactions, before and after the Cooling Process to 200 K^a

pressure contribution	before cooling (MPa)	after cooling (MPa)
kinetic	216 ± 1	111.5 ± 0.3
bond	$-(2.4 \pm 0.3) \cdot 10^2$	$-(3 \pm 2) \times 10^1$
valence angle	$\equiv 0$	$\equiv 0$
torsional angle	$\equiv 0$	$\equiv 0$
intermolecular	-10 ± 8	-73 ± 7
intramolecular	30 ± 4	-10 ± 2
total	0 ± 30	-0 ± 20

^{a} The data before cooling are the average values over the equilibration interval at 450 K, while those after cooling are average values over the interval from 4×10^4 MCS (counted from the moment the cooling was started) until the end of the "equilibration-after-cooling" process. The indicated error is the standard deviation of the distribution of all measured values. The total pressure hardly changes during the cooling, but the different contributions do change; whereas in the melt kinetic motion is balanced by bond stretching forces, in the glassy state nonbonded interactions (mainly intermolecular) keep the system stable.

rium quickly after 2×10^3 MCS. The equilibrium total energy is 22.1×10^3 kJ mol^{-1} (Figure 2b). The instantaneous pressure calculated in the present study is given in Figure 3, and the contributions to the pressure from different types of interactions are listed in Table 2. It is found that for the equilibrated PE sample in the melt state (450 K) negative contributions come from bond lengths and intermolecular nonbonded interactions, whereas a positive contribution comes from intramolecular nonbonded interactions. The fluctuations in the pressure, which are of the order of 30 MPa, are mainly caused by changes of the chemical bond lengths during volume fluctuation moves.

3.2. Cooling Process. After the equilibration at $T = 450$ K the cooling process is conducted by gradually cooling the PE sample down at a rate of 5×10^{-2} K MCS^{-1} to the final target temperature, followed by the equilibration at that temperature. The evolution of the instantaneous density and total energy in the cooling process from the melt temperature (450 K) to the three target temperatures, 100, 200, and 300 K is plotted in
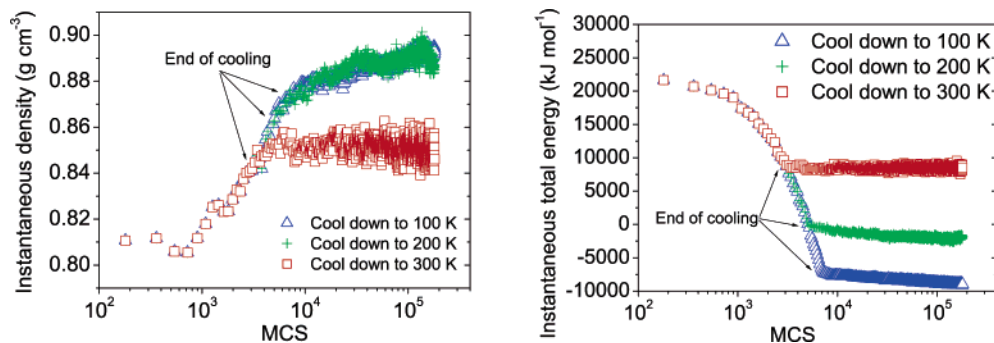
Figure 4. Evolution of the instantaneous density (left) and total energy (right) during the cooling process from 450 K to three lower temperatures. Results are plotted every 180 MCS. The sample which stays at the higher temperature shows the lower equilibrium density and higher equilibrium total energy. The slow relaxation processes at low temperatures require more than 2×10^5 MCS for the samples to be equilibrated.
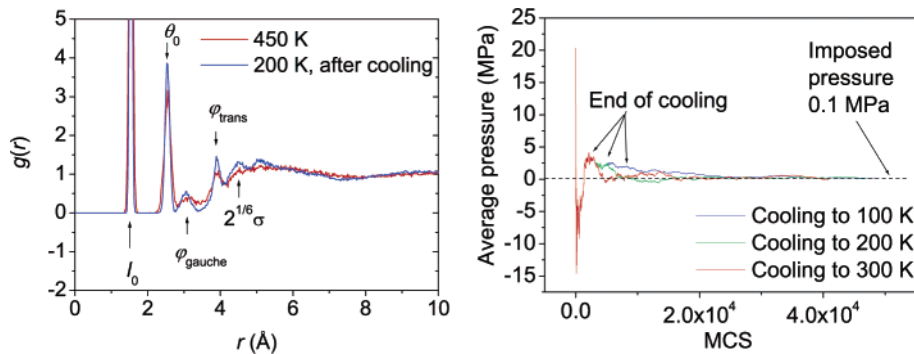

Figure 5. (Left) Pair correlation function for the equilibrium PE sample at 450 K and the PE glass at 200 K. The peaks corresponding to the equilibrium bond length l_0, the equilibrium bond angle θ_0, the gauche conformation ϕ_{gauche}, the trans conformation ϕ_{trans}, and the equilibrium nonbonded distance $2^{1/6}\sigma$ are indicated by arrows. (Right) Evolution of the average internal pressure during the cooling process and further aging. The results are plotted every 20 MCS. After the cooling has stopped, the internal pressure evolves in $\sim 10^4$ MCS to the value of the external pressure.
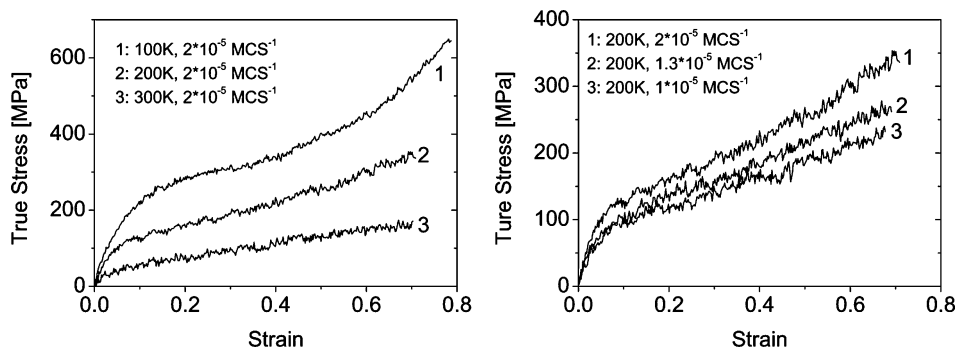

Figure 6. Stress−strain behavior during uniaxial deformation for various temperatures (left) and strain rates (right). A higher stress is observed for lower temperatures. Decreasing the strain rate results in a lower stress at fixed strain value. The initial elastic modulus is larger for lower temperature, but the moduli from different strain rates under the same temperature are close to each other.

Figure 4. In the cooling to 300 K the density quickly reaches the equilibrium value of 0.85 g cm^{-3} (4×10^3 MCS after the cooling stops), while the densities keep increasing as the cooling stops at 200 and 100 K. The evolution of the density during and after the cooling to these two low temperatures are very similar, suggesting a very slow relaxation at these temperatures. Probably the PE samples investigated in this study have a T_g in the range 200 K < T_g < 300 K (the experimental value equals 252 K[29]), and both samples (cooled to 200 and 100 K) are frozen in some amorphous states. The continuous decrease of the total energies after cooling to 200 and 100 K also indicates the slow structural relaxation process in these samples below T_g. We found that the changes of the internal structure during cooling are responsible for the large decrease of the total energy. These structural changes can be seen in Figure 5 (left) where the monomer−monomer pair correlation function before and after cooling to 200 K is plotted. Figure 5 (right) shows the average internal pressure (average of all values from the first move until

the last move performed) calculated from the atomic stress theorem (eq 1). The cooling process does not influence the consistency of the internal and the imposed pressures. However, the internal balance of different contributions does change; upon cooling, the intermolecular interactions instead of the intramolecular bond stretching start to play a dominant role in balancing the kinetic motion to keep the system stable, as shown in Table 2.

4. Uniaxial Deformation

4.1. Stress−Strain Behavior. The PE samples are uniaxially deformed at various temperatures and strain rates. The calculated (true) stress−strain relations are shown in Figure 6. Here the strain ϵ is defined as $(L_z - L_{z,0})/L_{z,0}$, with L_{z0} the box length prior to deformation. The calculated stresses (Figure 6) are higher than the typical stresses of high-density PE (HDPE), 10−50 MPa, observed in tensile experiments at room temperature.[30] That is probably because of the high deformation speed in the

Table 3. Young Moduli, Yield Stress, Yield Strain, and Strain Hardening Moduli of PE Glass Deformed at Various Temperatures and Strain Rates

T (K)	$\dot{\epsilon}$ (MCS^{-1})	E (MPa)	σ_y (MPa)	ϵ_y	G_R^ϵ (MPa)
100	2×10^{-5}	$(4.0 \pm 0.3) \times 10^3$	170 ± 2	0.06 ± 0.005	$(1.27 \pm 0.03) \times 10^3$
200	1×10^{-5}	$(1.3 \pm 0.2) \times 10^3$	90 ± 5	0.09 ± 0.005	$(2.5 \pm 0.3) \times 10^2$
200	1.3×10^{-5}	$(1.9 \pm 0.2) \times 10^3$	90 ± 5	0.07 ± 0.005	$(2.6 \pm 0.3) \times 10^2$
200	2×10^{-5}	$(2.5 \pm 0.2) \times 10^3$	115 ± 2	0.07 ± 0.005	$(4.2 \pm 0.3) \times 10^2$
300	2×10^{-5}	$(1.2 \pm 0.4) \times 10^3$	36 ± 2	0.05 ± 0.005	$(9 \pm 3) \times 10^1$

present simulations as compared to the experiments. Typically the strain rate used in experiments is about 0.1 s^{-1},[30] whereas the strain rate in the simulations is in the range of $(1 \times 10^{-5}-2 \times 10^{-5})$ MCS^{-1}. (As mentioned earlier, this corresponds to a strain rate of $\sim 10^8$ s^{-1}.) For clarity, the deformations take place at constant velocity; the deformation rates mentioned are the deformation rates at the start of the deformation. Apart from a difference in deformation velocity, a comparison with experimental observations is difficult because in reality PE is semicrystalline, whereas the sample used in our calculations is amorphous. Therefore, experimental values are only mentioned at a few instances in this paper, to give an idea to what extent the simulated material is or behaves different than real PE.

Because of the complications mentioned above, no attempt will be made to reproduce all experimental values, but on this point the aim is to show that the qualitative dependence of the stress−strain relation on temperature and strain rate can be obtained and to see how the results compare to those of previous simulation studies, e.g. by Capaldi et al.,[5] who report E moduli of order 2.5 GPa or by e.g. Brown and Clarke,[4] who observe an E modulus of 2.5 GPa at 100 K and half an order lower at room temperature. In the left panel of Figure 6 the stress−strain behavior for the temperatures at 100, 200, and 300 K at a strain rate of 2×10^{-5} MCS^{-1} can be seen. All curves show an initial elastic region (for strain values below 0.1), followed by yielding (the steep increase of stress with strain levels off at this point). The sample deformed at 100 K shows a clear transition to strain hardening at a strain of 0.5. The elastic deformation at small strains shows larger moduli for lower temperature samples. The elastic moduli, which are obtained from a linear fit to the stress−strain data for strains smaller than 0.02, are given in Table 3. These values are similar to the values found in other computational studies, e.g. by Brown and Clarke,[4] and for temperatures below T_g they are of the same order of magnitude as measured in the laboratory (of the GPa order[31]). At higher temperatures the moduli decrease by half an order of magnitude, which is far less than observed in experiments. These results can be understood by realizing that the material behaves elastic at low temperature, and therefore the deformation time scale is not relevant. For higher temperature the behavior is more viscous, and the time scale of deformation is deciding for the moduli. The yield point was determined as an intersection of the stress−strain curve with its tangent at zero strain (with slope equal to the E modulus) but shifted over 0.02 along the strain axis;[31] the values of the yield stress and yield strain are given in Table 3. These values are slightly higher than experimental values (for room temperature the yield stress is in the range 18−32 MPa[30]) but lower than values obtained in other simulations (for example, Capaldi et al.[21] find 200−300 MPa for deformation rates of $5 \times 10^9 - 5 \times 10^{10}$ s^{-1} at 200 K), which is probably due to the better equilibration of the present PE melts and to a lower deformation rate. Eventual strain hardening is caused by increased bond lengths and valence angles (as compared to their equilibrium values); see section 4.2. The strain-hardening moduli G_R^ϵ, obtained from a linear fit of the final parts of the stress−strain curves (final 10% of the deformation), are given in Table
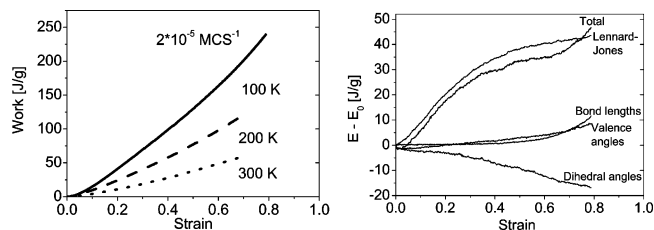

Figure 7. Work done at different temperatures and same strain rate $(2 \times 10^{-5}$ MCS$^{-1})$ (left) and the evolution of the internal energy contributions associated with bond lengths, bond angles, dihedral angles, and nonbonded interactions at 100 K and at a strain rate of 2×10^{-5} MCS^{-1} (right). E_0, which denotes the initial energy of a certain contribution before the deformation, is subtracted for clarity.

3 as well. These values are extremely high in comparison to typical experimental results (at room temperature the strain hardening moduli are typically in the range 1−5 MPa[30]), which probably means that the extent to which the bond lengths and valence angles are increased is unrealistic. The values are comparable to the values that can be extracted from previous simulation results reported by Capaldi et al.,[5] although they employed higher deformation rates.

In the right panel of Figure 6 the stress−strain relation is plotted for different strain rates $(1.0 \times 10^{-5}, 1.3 \times 10^{-5}$, and 2.0×10^{-5} MCS$^{-1})$ at the same temperature (200 K). The initial elastic moduli, the yield points, and the strain hardening moduli can be found again in Table 3. The Young modulus increases with the deformation velocity, which is probably an artifact of the measurement, in which the modulus is chosen as the slope of the stress−strain curve for deformation up to 2%; at 2% deformation the departure from nonlinear behavior is presumably too dramatic already at the higher strain rates. The yield stress and the strain hardening modulus also depend on the deformation velocity, but the dependencies are much weaker. Qualitatively, this picture is in agreement with the experimental[30] and computational[1,4,21] results mentioned before.

4.2. Evolution of Internal Energy Contributions and Stress Partitioning. To obtain insight into the molecular mechanisms at work during deformation of glassy amorphous PE, the evolution has been investigated of the various contributions to the internal energy from the bonded and nonbonded interactions at various stages of the deformation process, i.e., during initial linear-elastic response, yield, large deformation with low stress increase, and strain hardening. In addition, the contributions to the total stress have been studied. Finally, the influence of deformation on distributions of bond lengths, bond angles, and dihedral angles as well as on the intra- and intermolecular pair distribution functions has been investigated.

In Figure 7 (left panel) the work, calculated as the area under the stress−strain curve, done on the PE glass during deformation is given for three different temperatures. The applied work during deformation at room temperature is of the same order of magnitude as what is experimentally found.[20] The evolution of the internal energy during deformation at 100 K is shown in Figure 7 (right). It can be seen that for strain values below 0.4 a substantial part ($\sim$30%) of the mechanical energy is converted
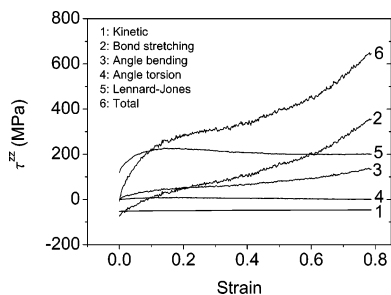
Figure 8. Stress partitioning in the sample during deformation: evolution of contributions from the different bonded and nonbonded interactions.

into internal energy of the sample, mainly as an increase of the nonbonded energy. At intermediate strain values (0.4−0.6) almost all energy is dissipated. At larger strain values (above 0.6) the mechanical energy is partly turned into internal energy related to conformational changes in the chains. At the final strain (0.8) about one-sixth of the applied work has been converted into internal energy. This is comparable to what is seen in experiments.[20] The energy from the Lennard-Jones interactions increases very fast up to the strain of 0.4 and then reaches a plateau, while the contributions from bonds and valence angles stay close to their initial values in the beginning and start to increase only after the strain of 0.5. The contribution from dihedral angles decreases during deformation, indicating a redistribution of dihedral angles, where the fraction of trans conformations increases.

The evolution of the different contributions to the stress τ^{zz} is shown in Figure 8. Initially, the nonbonded interactions are tensile (give a positive contribution to the stress of the system), whereas the bonded interactions are compressive (give a negative contribution to the stress of the system); more specifically, bond lengths give a compressive contribution, while bond angles and dihedral angles do not contribute. From a strain of 0.2 all contributions are tensile. (The only exception is the kinetic part of the stress, which is always compressive.) Upon deformation one observes initially a stiff response from both nonbonded and bonded interactions. As yielding sets in, the nonbonded contribution stops increasing, while the contribution from bonded interactions increases further at lower slope. Eventually, at strain values of 0.5−0.6, the contributions from bonded interactions, i.e., bond lengths and bond angles, start to increase more rapidly.

The above facts indicate that the deformation process can be divided in a few consecutive stages as follows:

Initially, in the elastic regime and slightly beyond (up to the strain of 0.1), the nonbonded interactions are dominant and bring the immediate response to the elongation.

Subsequently, as the deformation progresses, the amount of mechanical energy from the external load converted into nonbonded energy decreases to zero. Simultaneously, the bonded interactions become increasingly important in the response to the external loads. Dramatic changes of chain conformations occur. The probability densities of structural parameters before and at the end of the deformation at 100 K and at a strain rate of 2×10^{-5} MCS^{-1} are plotted in Figure 9. The unfolding of the chains results in the transformation of torsional angles from the gauche conformation to the trans conformation. The fraction of dyads in the trans conformation increases from 57% before deformation to 69% after deformation, as shown in Figure 9c, resulting in a decrease of the torsional energy. The decrease, after deformation, in the intensity of the peak at intramolecular distances $2^{1/6}\sigma$ and the increase of the peaks at higher values

(Figure 9d) indicates the transition of the chains to more extended conformations. The intermolecular distances shift to lower values. Apparently, the space previously occupied by intramolecular neighbors is now occupied by intermolecular neighbors.

Finally, at strain values larger than 0.5, the bond lengths and the bond angles start to absorb a considerable amount of energy and are responsible for a major contribution to the stress. This is the onset of strain hardening. It is clear from Figure 9a,b that the distributions of the bond lengths and the bond angles shift toward higher values during deformation, corresponding to higher energies.

Although for PE-like cross-linked networks a similar approach was followed already by Chui and Boyce,[1] to our knowledge this is the first study of the role of the different (separate) interactions during uniaxial deformation of an amorphous non-cross-linked PE-like glass. A comparison of the present paper with the results of Chui and Boyce is, though interesting, not without risk; apart from the topological differences (a cross-linked network vs a polymer melt) and the fact that Chui and Boyce study compression whereas the current paper concerns uniaxial extension, there are important differences in the PE force fields used in the two studies. Both Chui and Boyce and we use a Lennard-Jones potential for nonbonded interactions, but with different radii σ. Moreover, Chui and Boyce directly calculate 1−4 nonbonded interactions, whereas we account for 1−4 nonbonded interactions by including them in the dihedral potential. This difference makes comparison of both contributions from nonbonded interactions and dihedral interactions to energy and stress complicated. Presumably, it also explains why our results show tensile nonbonded interactions, whereas Chui and Boyce report compressive nonbonded interactions. Despite the differences, there are some similarities in the results; the initially stiff response to deformation of our PE-like polymer melt, followed by leveling off of the contribution of nonbonded interactions to the stress and a less steep increase of the bonded interactions, is also observed by Chui and Boyce.

The evolution of the density of the system during deformation is also examined for different temperatures at the same strain rate (2×10^{-5} MCS^{-1}) and for different strain rates at the same temperature (200 K). The sample deformed at 300 K, which is above T_g, shows initial dilation, after which the density fluctuates around a constant value during the rest of the deformation (see the left panel of Figure 10). At lower temperature the density keeps decreasing during the deformation, where the slope of the density curve increases with decreasing temperature. The influence of the strain rate is shown in the right panel of Figure 10: as the deformation rate decreases, the decrease of the density levels off and finally the density becomes constant. To facilitate a comparison with experimental results, use is made of the following ratio:

$$\mu = -\frac{\Delta L_\perp / L_\perp}{\Delta L_\| / L_\|} \qquad (2)$$

which is calculated after every 0.002 strain increase. $L_\|$ and $L_\perp$ are the instantaneous lengths of the sample along the elongation direction and the perpendicular direction, respectively, and $\Delta L_\|$ and $\Delta L_\perp$ denote the changes of the lengths $L_\|$ and $L_\perp$ since the last time the ratio was calculated. In the limit of zero strain, the ratio equals Poisson's ratio. At the lowest simulated temperature, 100 K (Figure 11), the value of Poisson's ratio is 0.34 ± 0.01, which is in the experimental range 0.3−0.4 [32] for a typical amorphous polymer. As yielding sets in, the ratio μ starts to
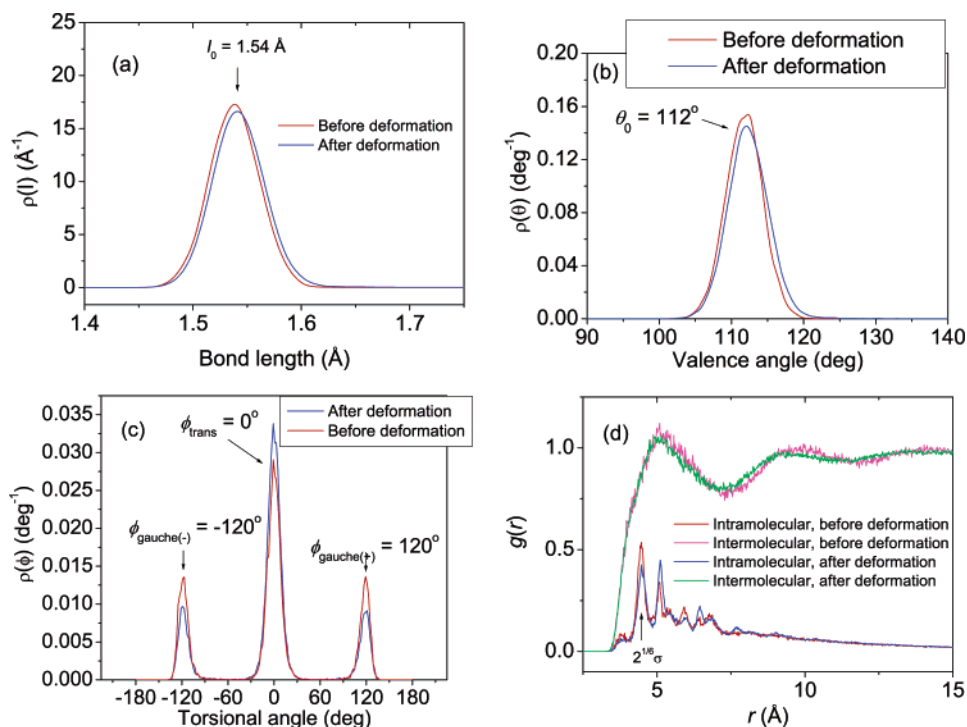
Figure 9. Comparison of the probability densities of (a) bond length, (b) valence angle, (c) torsional angle, and (d) nonbonded distance for the initial sample (before deformation) and the sample at the end of the deformation (after deformation) at 100 K and under a strain rate of 2×10^{-5} MCS^{-1}.
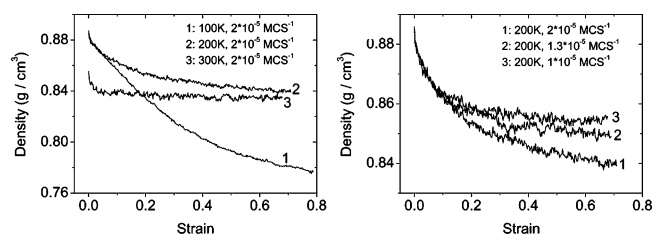

Figure 10. Density evolution during uniaxial deformation under different temperatures (left) and strain rates (right). All densities decrease; however, at lower temperature or at higher deformation velocity the decrease is more pronounced and continues up to larger strain. The initial samples equilibrated under different temperatures show different initial densities.
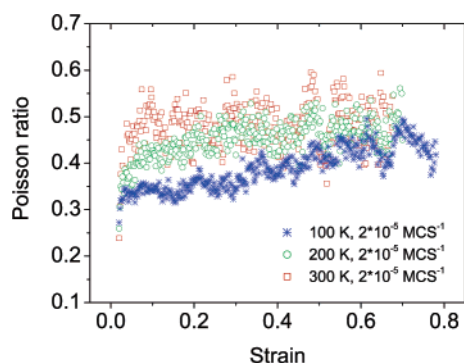

Figure 11. Evolution of Poisson ratio for the deformation at different temperatures (100, 200, and 300 K) and the same strain rate of 2×10^{-5} MCS^{-1}.

increase to 0.44 ± 0.03 at large strains, indicating that the rate at which the density decreases goes down. At the highest temperature, 300 K, the density is constant in a large range of strains, which is consistent with μ fluctuating around an average value of 0.48 ± 0.04 during the deformation and with a picture of local incompressible flow.

5. Conclusions

MC simulations have been performed of the uniaxial deformation of an amorphous PE-like polymer glass. A united-atom representation is used for the structure of PE. The MC algorithms used in the equilibration at the melt temperature are extensively described by Theodorou et al.[13,14] and include local moves (flips, end and concerted rotations) as well as reptation and connectivity-altering end-bridging moves. Especially the last two moves are important in order to produce well-equilibrated polymer samples before deformation is applied. By changing the connectivity of polymer chains, the mechanisms associated with the longest relaxation times are circumvented. After cooling to a temperature near or below T_g, uniaxial deformation of the equilibrated PE glass was performed by constant-velocity elongation at different temperatures, using partly the same MC moves.

The results of the present study show that the extension of the MC algorithms of Theodorou et al. to uniaxial deformation provides a new approach for studying the mechanical behavior of model polymer systems.

The stress−strain behavior we obtained shows the typical transitions from the elastic deformation in the beginning, to yield, then to large deformation with low stress increase, and finally to strain hardening (even for the unentangled systems considered here), as observed in experiments. We also qualitatively reproduced the dependencies of the PE stress−strain behavior on temperature and strain velocity, where stress at the same strain was larger for lower temperatures and higher strain velocities. Moreover, despite the large deformations in our simulations, realistic values are found for E-moduli, yield stresses, and Poisson ratios. The evolution of the internal energy and chain conformations during the mechanical deformation indicate that the deformation process can be divided in a few consecutive stages as follows: In the elastic regime and slightly beyond (up to a strain of 0.1) the nonbonded interactions are dominant and density decreases. As the deformation progresses,

the amount of mechanical work converted into the nonbonded energy decreases to zero, whereas the bonded interactions become increasingly important in the response to the external load. Chain conformations change considerably under deformation, while the density decrease diminishes. The unfolding of the chains results in the transformation of torsional angles from the gauche conformation to the trans conformation and a decrease of the torsional energy. The fraction of the trans conformations increases from 57% prior the deformation to 69% after deformation, resulting in a decrease of the total torsional energy. Changes in both the intra- and interchain pair correlation functions imply a transition after yield to local flow of densely packed chains in more extended conformations. Strain hardening is observed at strain values larger than 0.5, where the chemical bonds and the valence angles start to absorb a considerable amount of energy and are responsible for a major contribution to the total stress.

References and Notes

(1) Chui, C.; Boyce, M. C. *Macromolecules* **1999**, *32*, 3795−3808.
(2) Arruda, E. M.; Boyce, M. C. *Int. J. Plast.* **1993**, *9*, 697−720.
(3) Melick, H. G. H. Deformation and failure of polymer glasses. Ph.D. Thesis, Technische Universiteit Eindhoven, 2002.
(4) Brown, D.; Clarke, J. H. R. *Macromolecules* **1991**, *24*, 2075−2082.
(5) Capaldi, F. M.; Boyce, M. C.; Rutledge, G. C. *Polymer* **2004**, *45*, 1391−1399.
(6) Lyulin, A. V.; Vorselaars, B.; Mazo, M. A.; Balabaev, N. K.; Michels, M. A. J. *Europhys. Lett.* **2005**, *71*, 618−624.
(7) Ogura, I.; Yamamoto, T. *Polymer* **1995**, *36*, 1375−1381.
(8) Lyulin, A. V.; Balabaev, N. K.; Mazo, M. A.; Michels, M. A. J. *Macromolecules* **2004**, *37*, 8785−8793.
(9) Vacatello, M.; Avitabile, G.; Corradini, P.; Tuzi, A. *J. Chem. Phys.* **1980**, *73*, 548−552.
(10) Siepmann, J. I.; Frenkel, D. *Mol. Phys.* **1992**, *75*, 59−70.
(11) Dodd, L. R.; Boone, T. D.; Theodorou, D. N. *Mol. Phys.* **1993**, *78*, 961−996.
(12) Dodd, L. R.; Theodorou, D. N. *Adv. Polym. Sci.* **1994**, *116*, 249−281.
(13) Mavrantzas, V. G.; Boone, T. D.; Zervopoulou, E.; Theodorou, D. N. *Macromolecules* **1999**, *32*, 5072−5096.
(14) Pant, P. V. K.; Theodorou, D. N. *Macromolecules* **1995**, *28*, 7224−7234.
(15) Wittkop, M.; Sommer, J. U.; Kreitmeier, S.; Goritz, D. *Phys. Rev. E* **1994**, *49*, 5472−5476.
(16) Hölzl, T.; Mesner, C.; Kreitmeier, S.; Goritz, D. *Comput. Theor. Polym. Sci.* **1999**, *9*, 99−109.
(17) Ospina, S. A.; Restrepo, J.; Lopez, B. L. *Mater. Res. Innov.* **2003**, *7*, 27−30.
(18) Ospina, S. A.; Hess, M.; Lopez, B. L. *e-Polym.* **2004**, no. 024.
(19) Brostow, W.; Corneliussen, R. D. *Failure of Plastics*; Hanser: New York, 1986.
(20) Hasan, O. A.; Boyce, M. C. *Polymer* **1993**, *34*, 5085−5092.
(21) Capaldi, F. M.; Boyce, M. C.; Rutledge, G. C. *Phys. Rev. Lett.* **2002**, *89*, 175505.
(22) Ryckaert, J. P.; Bellemans, A. *Chem. Phys. Lett.* **1975**, *30*, 123−125.
(23) Theodorou, D. N.; Suter, U. W. *Macromolecules* **1985**, *18*, 1467−1478.
(24) Allen, M. P.; Tildesley, D. J. *Computer Simulation of Liquids*; Clarendon Press: Oxford, England, 1987.
(25) Theodorou, D. N.; Boone, T. D.; Dodd, L. R.; Mansfield, K. F. *Makromol. Chem. Theory Simul.* **1993**, *2*, 191−238.
(26) Smith, W. *CCP5 Info. Q.* **1993**, 14−21.
(27) Karayiannis, N. C.; Giannousaki, A. E.; Mavrantzas, V. G.; Theodorou, D. N. *J. Chem. Phys.* **2002**, *117*, 5465−5479.
(28) Paul, W.; Smith, G. D.; Yoon, D. Y. *Macromolecules* **1997**, *30*, 7772−7780.
(29) Bandrup, J.; Immergut, E. H. *Polymer Handbook*; J. Wiley and Sons: New York, 1966.
(30) Kennedy, M. A.; Peacock, A. J.; Mandelkern, L. *Macromolecules* **1994**, *27*, 5297−5310.
(31) Ward, I. M.; Sweeney, J. *An Introduction to the Mechanical Properties of Solid Polymers*; J. Wiley and Sons: Chichester, England, 2004.
(32) McKechnie, J. I.; Haward, R. N.; Brown, D.; Clarke, J. H. R. *Macromolecules* **1993**, *26*, 198−202.